A time dependent phase space filter for anisotropic wave equations on unbounded domains

Thomas Hagstrom [*], Dinh Phan Cao Nguyen [†], Avy Soffer [‡]
Chris Stucchio [§], Minh-Binh Tran [¶]

March 2, 2025

Abstract

For wave propagation problems in homogeneous, isotropic media exponentially-convergent domain truncation techniques based on perfectly-matched damping layers or optimal rational approximations to the exact radiation operator are known. However these methods fail for systems with wave families satsfying general dispersion relations, forcing practitioners to resort to ad hoc procedures based on grid stretching and artificial damping. Here we propose a new method for constructing convergent approximations on truncated domains, the phase space filter, which unlike other methods is completely general and mathematically-justified. Based on the fact that outgoing waves can be characterized as waves located near the boundary of the computational domain with group velocities pointing outward, the key idea of the phase space filtering algorithm consists of applying a filter to the solution that removes outgoing waves only. The method introduced in this work is a simplified version of the original phase space filter, originally proposed in [34] for the Schrödinger equation. The method is applied to anisotropic wave models for which existing techniques unstable, namely free space problems governed in the far field by the Euler equations linearized about a uniform mean flow and Maxwell's equations in an anisotropic medium. Theoretical results concerning the convergence and computational costs of the phase space filter are discussed and stability is proven.

[1]Department of Mathematics, Southern Methodist University, Dallas, TX 75275, USA.
TH is funded in part by NSF Grant DMS-2309687. Any opinions, findings, and conclusions or recommendations expressed in this material are those of the authors and do not necessarily reflect the views of the National Science Foundation.
[2]Faculty of Information Technology, Nha Trang University, Vietnam.
[3]Mathematics Department, Rutgers University, New Brunswick, NJ 08903 USA.
[4]Mathematics Department, Rutgers University, New Brunswick, NJ 08903 USA.
[5]Department of Mathematics, Texas A&M University, College Station, TX 77843, USA.
M.-B. T is funded in part by is funded in part by a Humboldt Fellowship, NSF CAREER DMS-2303146, and NSF Grants DMS-2204795, DMS-2305523, DMS-2306379.

1 Introduction

We consider the solution of linear wave equations of the form:

$$\vec{u}_t(\vec{x},t) = \mathcal{H}\vec{u}(\vec{x},t) \tag{1.1}$$

Here, $\vec{u} : \mathbb{R}^N \to \mathbb{R}^n$ (or $\mathbb{R}^N \to \mathbb{C}^n$) and $\mathcal{H}$ is a skew-adjoint linear differential operator. This is a prototypical example of a linear wave equation. Such equations admit linear waves of the form $e^{i(\vec{k}\cdot\vec{x}-\omega_j(\vec{k})t)}\vec{d}_j(k)$ with $\vec{d}_j(\vec{k})$ the j'th eigenvector of $\mathcal{H}$ and $\omega_j(\vec{k})$ the j-th eigenvalue of $\mathcal{H}$ in the frequency domain. In particular we wish to solve numerically problems which are governed by (1.1) exterior to some finite region $B \subset \mathbb{R}^N$, possibly with scatterers, potentials, or even nonlinear effects confined to B.

A great many systems of practical importance can be recast in such a form, including the wave equation, Schrödinger's equation, and, as considered here, symmetrizable hyperbolic systems. For an important subclass of such systems, in particular isotropic systems where the directions of the phase and group velocity point in the same direction, exponentially-convergent domain truncation methods are available. Most popular among these is the so-called perfectly matched layer (PML). Introduced as a numerical method for Maxwell's equations by Bérenger [8], the original PML can be interpreted as complex coordinate stretching [11] or more generally as a rational transformation of the dispersion relation [4]. (The complex stretching technique was used in scattering theory for a long time [16, 33].) An even more efficient local method can be built from optimal rational approximations to the exact non-reflecting boundary conditions (NRBCs), the complete radiation boundary conditions (CRBC) introduced in [21]. However, these efficient methods are not general. For certain types of anisotropic waves, the PML can become exponentially unstable in time regardless of the particular method used (the instability exists on the level of the PDE). This was first noticed in [23] for the Euler equations linearized about a mean flow (see also [5, 6] for other examples). In [5], a simple geometrical criterion[1] was provided for a PML to be unstable. This instability occurs because the PML shifts the spectrum of the Hamiltonian into the upper half plane. Similarly, the convergence argument for CRBC fails in the same cases where the geometric criterion in [5] applies, and it seems clear that only by entering the realm of matrix-valued rational approximations is there any possibility of making CRBC generally applicable.

There have been somewhat successful attempts to extend PML [17, 14, 22, 9] and high-order approximate boundary conditions [20, 7, 19, 18] to time-dependent anisotropic problems or cases where the geometric criterion applies. However, these have generally been limited to problems with only a single wave family, such as scalar problems or Maxwell's equations in dispersive media, or reliant on underresolution to suppress the instabilities. Generalizations to the linearized Euler equation have worked in duct geometries, but attempts to

[1] There are some other conditions necessary for the proof to apply, but it is convincingly argued that this is the fundamental criteria.

use them in free space have required ad hoc stabilizations [27]. In principle, temporally-localized, spatially nonlocal approximations should be applicable to general problems, but to date their use has been limited to isotropic problems [1, 2, 24, 25, 26] or in one space dimension [15]. The only general approach, aside from the one developed here, is the use of ad hoc damping layers. Although, as shown in [3], the method can effectively treat problems for which PML is unstable, it is tied to particular discretizations and lacks analysis in the continuous setting.

In [34] an alternative and new approach to the problem of open boundaries was introduced, the Time Dependent Phase Space Filter (TDPSF). Phase space analysis is a major tool in modern scattering theory [30, 31, 32]. The key idea in this approach is that certain regions of quantum phase space (the set of points $\{(\vec{x},\vec{k}) \in \mathbb{R}^N \times \mathbb{R}^N\}$, where $\vec{x}$ represents a position and $\vec{k}$ a spatial frequency) consist solely of outgoing waves, whereas other regions have more complicated interactions. The philosophy of the TDPSF is to identify parts of the solution $\vec{u}(\vec{x},t)$ localized in the outgoing regions of phase space, and filter them from the solution before they reach the boundary. After these waves are filtered, $\vec{u}(\vec{x},t)$ is not approaching the boundary, and therefore boundary conditions don't matter.

In [34, 35, 36], this approach is used to construct open boundaries for the Schrödinger equation. The phase space projections there are based on the Gaussian windowed Fourier transform [12]. In this paper, we extend the work of [35, 34] to symmetrizable hyperbolic (Friedrichs) systems. We also simplify the method significantly, replacing the windowed Fourier transform by standard phase space projections of the form $\chi(\vec{x})P(k)\chi(\vec{x})$ (this approach was also taken in [35]). We begin by briefly reviewing the dynamics of linear waves (Section 1.1) and note its applicacion to they hyperbolic case. In Section 2 we present the phase space filtering algorithm for general systems of the form (1.1). In Section 3, we show some numerical examples. In Section 4, we briefly discuss a method of filtering outgoing waves with frequencies too small to resolve on an absorbing boundary layer of reasonable width.

1.1 Dynamics of Waves

For concreteness and to pin down our notation, we review a few facts about wave propagation. Recall that we defined $\omega_j(\vec{k})$ as the k'th branch of the dispersion relation, and $\vec{d_j}(\vec{k})$ as the corresponding normalized eigenvector. With this notation, $e^{i(\vec{k}\cdot\vec{x}-\omega_j(k)t)}d_j(\vec{k})$ is a standard plane wave solution of (1.1).

Let us define the matrix D to be the (unitary) matrix with j'th row $\vec{d_j}(k)$. This matrix can be used to diagonalize $\mathcal{H}$, i.e:

$$\mathcal{H} = D^\dagger \begin{bmatrix} i\omega_1(\vec{k}) & \dots & 0 \\ \dots & i\omega_j(\vec{k}) & \dots \\ 0 & \dots & i\omega_n(\vec{k}) \end{bmatrix} D \tag{1.2}$$

Let $e^{\mathcal{H}t}$ denote the propagation operator for (1.1), i.e. the operator mapping

$\vec{u}(x,0)$ to $\vec{u}(x,t)$. In the frequency domain, the propagator can be written as:

$$e^{\mathcal{H}t} = D^\dagger \exp\left(\begin{bmatrix} i\omega_1(\vec{k}) & \dots & 0 \\ \dots & i\omega_j(\vec{k}) & \dots \\ 0 & \dots & i\omega_n(\vec{k}) \end{bmatrix} t \right) D \tag{1.3}$$

Now consider an initial condition $\vec{u}_0(x)$ localized in frequency about the point $\vec{k}_0$ and in position about the point $\vec{x}_0$. Consider the solution $\vec{u}(x,t)$ with $\vec{u}(x,t=0) = \vec{u}_0(x)$. This solution can be written in the frequency domain as:

$$\begin{aligned} \widehat{\vec{u}}(\vec{k},t) &= e^{\mathcal{H}t}\vec{u}_0(x)\widehat{\vec{u}}_0(\vec{k}) \\ &= D^\dagger \exp\left(\begin{bmatrix} i\omega_1(\vec{k}) & \dots & 0 \\ \dots & i\omega_j(\vec{k}) & \dots \\ 0 & \dots & i\omega_n(\vec{k}) \end{bmatrix} t \right) \begin{pmatrix} u^1(\vec{k}) \\ \dots \\ u^n(\vec{k}) \end{pmatrix} \end{aligned} \tag{1.4}$$

where $u^j(\vec{k})$ is the projection of $\widehat{\vec{u}}_0(\vec{k})$ onto $\vec{d}_j(\vec{k})$ and $\widehat{f}(\vec{k})$ denotes the Fourier transform of $f(\vec{x})$.

The j-th component corresponds to a superposition of plane waves propagating with velocity $\nabla_k \omega_j(\vec{k})$. If we consider only regions of $\vec{k}$-space in which $\partial_{k_1}\omega_j(\vec{k}) > 0$, then we are considering only waves with a rightward moving component. The same can be said about other directions. It is this property combined with phase space localization techniques which we will use to filter outgoing waves.

Our focus here is on symmetrizable hyperbolic systems:

$$T\vec{u}_t(\vec{x},t) = \sum_j A_j \vec{u}_{x_j}(\vec{x},t) + B\vec{u}, \tag{1.5}$$

where $T = T^T > 0$, $A_j = A_j^T$, and $B^T = -B$. We put the system in the form (1.1) with the transformation $\vec{u} \to T^{1/2}\vec{u}$, $A_j \to T^{-1/2}A_jT^{-1/2}$, $B \to T^{-1/2}BT^{-1/2}$, and henceforth assume this has been done. (That is $T = I$.) Then the dispersion relations correspond to real algebraic varieties

$$\det\left(\omega_j(\vec{k}) + \sum_\ell k_\ell A_\ell - iB \right) = 0,$$

and the group velocity $\nabla_k\omega_j(\vec{k})$ is well-defined except possibly at exceptional points, which at worst form a subvariety of lower dimension [29, Ch. 2]. We will assume that such points are not encountered, as will be the case for our examples. We also recall that hyperbolic systems have finite speed of propagation and denote by $v_{\max}$ the largest group velocity:

$$v_{\max} = \sup_j \sup_{\vec{k}} \left| \nabla_k \omega_j(\vec{k}) \right| \tag{1.6}$$

2 Method

The methodology of the phase space filter is rather simple. First, given the operator $\mathcal{H}$, we find the generalized eigenfunctions and the dispersion relation. Suppose that the dispersion relations $\omega_j(\vec{k})$ and $\vec{d}_j(\vec{k})$ are given. If this is the case, then $\vec{d}_j(\vec{k})$ is a plane wave propagating with group velocity $\nabla_k \omega_j(\vec{k})$.

2.1 The Propagation Algorithm

The propagation algorithm is simple. Fix a time $T_{\text{step}} \leq w/3v_{\max}$, with being the the largest group velocity relevant to the problem. This criterion ensures that waves cannot cross the buffer region in a time interval shorter than T_{step}.

On the time intervals $[0, T_{\text{step}}]$, $[T_{\text{step}}, 2T_{\text{step}}]$, ..., we solve (1.1) with the interior propagator. At times T_{step}, $2T_{\text{step}}$, ..., we apply outgoing wave filters $\mathcal{O}_j^{\pm}$ (defined in the next section) to the regions $[-L-w, L+w]^N \backslash [-L, L]^N$. After the application of this filter, all propagating waves which would have reached the boundary before a time T_{step} have been removed, and we simply apply a stable boundary condition.

Algorithm 2.1 *TDPSF Propagation Algorithm*
Given an initial condition $\vec{u}_0(x)$, this algorithm calculates $\vec{u}_d(x,t)$.

***Input**:*

- *The dispersion relations and diagonalizing matrices, $\omega_j(\vec{k})$ and D.*
- *$e^{\mathcal{H}_b t}$, a propagator that accurately solves the interior problem.*
- *$k_{\max}$, the maximal frequency of the problem.*

1. *Define $T_{\text{step}} = w/3v_{max}$.*
2. *Define the approximate solution $\vec{u}_d(x,t)$ recursively. At times which are an integer multiple of T_{step}, we filter off the outgoing waves:*

$$\vec{u}_d(x,(m+1)T_{\text{step}}) = \left[\prod_{j=1}^{N}(1-\mathcal{O}_j^+)(1-\mathcal{O}_k^-)\right] e^{\mathcal{H}_b T_{\text{step}}} \vec{u}_d(x, mT_{\text{step}}) \tag{2.1a}$$

The outgoing wave filters are computed using Algorithm 2.2, described in Section 2.2.

For other times, we use the given interior propagator:

$$\vec{u}_d(x, mT_{\text{step}} + \tau) = e^{\mathcal{H}_b \tau} \vec{u}_d(x, mT_{\text{step}}) \text{ for } \tau \in [0, T_{\text{step}}) \tag{2.1b}$$

$$\vec{u}_d(x,0) = \vec{u}_0(x) \tag{2.1c}$$

It now remains to construct the outgoing wave filters, $\mathcal{O}_j^{\pm}$.

2.2 Construction of the boundary filter

Consider a fixed boundary region, say the boundary at $\vec{x}_1 = L$. For a frequency $\vec{k}$, if $\partial_1 \omega_j(\vec{k}) > 0$, then waves with frequency $\vec{k}$ are outgoing at this boundary. The outgoing region of phase space at the right boundary is therefore

$$\{(\vec{x}, \vec{k}) \in \mathbb{R}^N \times \mathbb{R}^N : \vec{x}_1 > L \text{ and } \partial_1 \omega_j(\vec{k}) > 0\}. \tag{2.2}$$

We now construct a projection onto this region. The Heisenberg uncertainty principle makes an exact projection impossible, but we will do the best it allows.

Extend the box a width w, to be specified shortly. Define the function

$$\chi_j^{\pm}(x) = \left(\frac{1}{\sigma\sqrt{\pi}}\right)^N e^{-\vec{x}^2/\sigma^2} \star I_j(x) \tag{2.3}$$

where $I_j(x) = 1$ for $x_j \in [\pm(L + w/3), \pm(L + 2w/3)]$ and $x_k \in [-L - 2w/3, L + 2w/3]$ (for $k \neq j$), and 0 elsewhere. The parameter $\sigma = O(w/\ln(\delta^{-1})^{1/2})$; a precise bound is given in (2.7). This ensures that $\chi_j^{\pm}(x) < \delta$ for $x_j \notin [\pm L, \pm(L + w)$ or $x_k \notin [-L - w, L + w]$. This function is smooth, and well localized inside the buffer region on the j'th sides of the box.

The set $R_{j,l} = \{\vec{k} \in \mathbb{R}^N : \partial_{k_j} \omega_l(\vec{k}) > 0\}$ is the set of frequencies with the k'th branch of the group velocity pointing right. Due to the Heisenberg uncertainty principle, we cannot project onto this set precisely. However, we can approximately project onto most of these wave-vectors. Define

$$R_{j,l,\delta} = \{\vec{k} \in R_k : d(\vec{k}, R_{j,l}^C) > k_b\} \tag{2.4a}$$

The set of vectors within a distance k_b of group velocity $\partial_{k_j} \omega_l(x) = 0$ is the set of group velocities with motion normal to side j approximately equal to zero. The width k_b is a buffer to ensure that the frequency spreading caused by our spatial localization operators does not cause an error larger than δ. Given k_b, we must also choose $\sigma \geq O({k_b}^{-1} \ln(\delta^{-1})^{1/2})$ to ensure that the spatial localization operators do not spread the frequency content of the solution past the buffer region of width k_b. Neglecting these waves causes an error if the simulation time is long enough for them to reach the boundary of the buffer zone. In this case, we must assume that

$$\int_{\{\vec{k} \in R_k : d(\vec{k}, R_{j,l}^C) \leq k_b\}} \left|\widehat{\vec{u}}_0(\vec{k})\right|^2 d\vec{k} \leq \delta \tag{2.4b}$$

This difficulty can be resolved at logarithmic cost, and this is discussed briefly in Section 4.

In particular, as shown below, we must choose the buffers widths k_b, w and standard deviation σ to satisfy

$${k_b}^{-1} \left(\ln(\delta^{-1}) + \ln\left(\frac{w^2 L^{N-1} \sigma^{3N}}{\pi^{3N/2}}\right)\right)^{1/2} \leq \sigma \leq \frac{w}{3\sqrt{\left|\ln 3\delta\sigma\pi^{1/2}/w\right|}}, \tag{2.4c}$$

which ensures that spreading in frequency does not turn waves around (thus minimizing reflection). This is estimated in Section 2.2.1. In particular, note that (2.4c) implies the buffer width w must be at least $O({k_b}^{-1}\ln(\delta^{-1}))$ (as expected from the Heisenberg uncertainty principle).

The frequency projection operator is defined as:

$$P_{j,l,\delta}(k) = \left(\frac{\sigma}{\sqrt{\pi}}\right)^N e^{-k^2\sigma^2} \star \begin{bmatrix} 1_{R_{j,l,\delta}}(\vec{k}) & \dots & 0 \\ \dots & 1_{R_{j,l,\delta}}(\vec{k}) & \dots \\ 0 & \dots & 1_{R_{j,n,\delta}}(\vec{k}) \end{bmatrix} \tag{2.4d}$$

Thus, the operator $P_{j,l,\delta}(k)$ is a smooth projection (in the basis of eigenvectors of $\mathcal{H}$) onto wave-vectors propagating rightward. Conjugation of $P(\vec{k})$ by D moves the projection into the domain of frequency vectors. Finally, we define the operator:

$$\mathcal{O}_1^+ = \chi_1^+(x) D^\dagger P(\vec{k}) D \chi_1^+(x) \tag{2.5}$$

This operator both localizes in the buffer region at $x = L$, and projects onto waves with group velocity pointing to the right. This operator can be computed efficiently and with spectral accuracy as follows:

Algorithm 2.2 *Outgoing Wave Filter Algorithm*

This algorithm applies the outgoing wave filters, i.e. it numerically approximates $(1 - \mathcal{O}_j^\pm)\vec{u}(x)$.

Input:

- *The dispersion relations and diagonalizing matrices,* $\omega_j(\vec{k})$ *and* D.
- *A function* $\vec{u}(x)$.
- *Indices* $(j, \cdot)$ *with* $j \in 1 \dots n$ *and* $\cdot \in \{+, -\}$.

We assume that the operator $D^\dagger P(\vec{k}) D$ *is precomputed.*

1. *Compute the function* $\chi_j^\pm(x)\vec{u}(x)$*, and take it's Fast Fourier Transform.*
2. *Apply* $D^\dagger P(\vec{k}) D$ *to the Fast Fourier transform of* $\chi_j^\pm(x)\vec{u}(x)$.
3. *Apply the inverse Fast Fourier Transform, and multiply the result by* $\chi_j^\pm(x)$.
4. *Subtract the result from* $\vec{u}(x)$*, and return the result.*

2.2.1 Choosing the Buffer Widths

The buffer widths, w and k_b must be chosen carefully for this algorithm to work. There are two competing concerns, namely width of the buffer region and frequency spreading, which we must address at this point.

If w is too small, then the spatial localization functions $\chi_j^{\pm}(x)$ will become rougher. But roughness in $\chi_j^{\pm}(x)$ will spread the frequencies of the solution around. In the frequency domain, multiplication by $\chi_j^{\pm}(x)$ corresponds to convolution, and behaves much like a diffusion operator in the k variable. The danger is that the diffusion in k might move mass from the region with positive group velocity to the region with negative group velocity.

However, a larger w will increase the size of the computational box, and therefore the computational complexity of the method. Thus, it is desirable to take w as small as possible.

We analyze this as follows. Multiplication by $\chi_j(x)$ corresponds (in the k-domain to convolution with[2] $(wL^{N-1}/3)(\sigma^N\pi^{-N/2})e^{-k^2\sigma^2}$. Thus, we can approximate the frequency domain operations by:

$$(wL^{N-1}/3)(2^N\sigma^N\pi^{-N/2})e^{-k^2\sigma^2} \star (wL^{N-1}/3)(\sigma^N\pi^{-N/2})e^{-k^2\sigma^2}\star \\ = w^2L^{N-1}\sigma^{2N}\pi^{-N}e^{-k^2\sigma^2/2}\star$$

The frequency domain operators $P_{j,l,\delta}(\vec{k})$ are localized on the regions $R_{j,k,\delta}$, also with a Gaussian tail of the form $(\sigma\pi^{-1/2})^N e^{-k^2\sigma^2}$.

The region $R_{j,l,\delta}$ is separated from the region containing incoming waves by a buffer of width k_b. We want to make sure that the spreading in frequency is small past this buffer of width k_b, i.e.:

$$w^2L^{N-1}\sigma^{2N}\pi^{-N}e^{-k^2\sigma^2/2} \star (\sigma\pi^{-1/2})^N e^{-k^2\sigma^2}\Big|_{|\vec{k}|=k_b} \leq \delta$$

This can be guaranteed by:

$$k_b{}^{-1}\left(\ln(\delta^{-1}) + \ln\left(\frac{w^2L^{N-1}\sigma^{3N}}{\pi^{3N/2}}\right)\right)^{1/2} \leq \sigma \tag{2.6}$$

On the other hand, if we take σ too large, then the tails of $\chi_j^{\pm}(\vec{x})$ will enter the computational domain. To ensure that this is minimized, we want to make certain that $\chi_j^{\pm}(\vec{x}) \leq \delta$ for $\vec{x} \in [-L, L]^N$. By examining the form of (2.3), we find that this can be accomplished if

$$\frac{1}{\sigma\sqrt{\pi}}\int_{w/3}^{2w/3} e^{-x^2/\sigma^2}dx \leq \frac{w}{3\sigma\sqrt{\pi}}e^{-w^2/(9\sigma^2)} < \delta,$$

which implies

$$\sigma \leq \frac{w}{3\sqrt{\left|\ln 3\delta\sigma\pi^{1/2}/w\right|}}. \tag{2.7}$$

[2]We have suppressed the sinc(...)-factor corresponding to the Fourier transform of $I_j(x)$, just for simplicity. This is an overestimate.

Additionally, to satisfy simultaneously (2.6) and (2.7), we must have that:

$$k_b{}^{-1}\left(\ln(\delta^{-1})+\ln\left(\frac{w^2L^{N-1}\sigma^{3N}}{\pi^{3N/2}}\right)\right)^{1/2}\leq\frac{w}{3\sqrt{\left|\log 3\delta\sigma\pi^{1/2}/w\right|}}. \tag{2.8}$$

This condition demands essentially that $w \geq Ck_b{}^{-1}$, where $C = O(\ln(\delta^{-1}))$, which is what we should expect based on the Heisenberg uncertainty principle.

2.3 Computational Cost and Implementation Details

The computational cost of the proposed method is determined primarily by the width of the extended buffer region. This, in turn, is determined by the frequency range of the problem.

The cost of a filtering operation is the cost of performing an FFT on the buffer region. This region has volume $w \cdot L^{N-1}$ with sampling rate $O(k_{\max}^N)$ for a total of $O(k_{\max}^N w L^N)$ lattice points. By rearranging (2.8), we find that the filter width scales like:

$$\text{Filter width} = w = O(k_{\min}^{-1}(\ln(\delta^{-1}) + \ln(L))) \tag{2.9}$$

When $k_{\min}^{-1} \ll L$, then the buffer width is small compared to the size of the box. We conjecture that the logarithmic dependence on L is merely an artifact of our calculation techniques. We thus find that the complexity of a single filtering operation (on one side of the box) is:

$$\begin{aligned}\text{Cost of one filtering} &= O(n\log(n)) &\text{(2.10a)}\\ n &= O\left[k_{\min}^{-1}k_{\max}^N L^{N-1}(\ln(\delta^{-1})+\ln(Lw))\right] &\text{(2.10b)}\end{aligned}$$

In particular, this implies that the added computational cost of the boundary filter depends only logarithmically on the size of the computational domain.

The filtering must then be performed $2N$ times, once for each side of the box, every $T_{\text{step}} \leq w/3v_{\max}$. Thus, the added complexity of the filtering operation is:

$$\text{Filtering cost} = O\left(2N\frac{T_{\max}v_{\max}}{w}n\log(n)\right) \tag{2.10c}$$

This additional cost is small in the regime $k_{\min}^{-1} \ll L$, i.e. the regime where the longest wavelengths relevant to the problem are small compared to the size of the computational domain.

2.3.1 Powers of 2

As a practical matter, there is an additional constraint on the buffer width. The projections onto outward moving group velocities (the $D^\dagger P(\vec{k})D$ part of $\mathcal{O}_j^\pm$) are performed using an FFT, which is fastest when performed on a grid of size 2^m in each dimension. For this reason, it is efficient to take $w = 2^m\delta x$ with $m = \lceil \log_2(w_{min}/\delta x)\rceil$. Here, w_{min} is minimal w satisfying (2.8) and δx is the lattice spacing in position. This does not affect the computational complexity (in terms of Big-O), though it can impose substantial additional costs in practice.

2.3.2 Implementation Details

Programming a phase space filter is a reasonably straightforward matter, and most existing codes can be adapted to use them. Given an existing time-stepping program for solving (1.1), one simply needs to stop the simulation at $t = T_{\text{step}}, 2T_{\text{step}}, \ldots$, apply the phase space filter, and continue. The main requirements made by the phase space filter is that δt, the timestep of the existing code, satisfies $\delta t < T_{\text{step}}$. Since $T_{\text{step}} < O(w/v_{\max})$ while $\delta t < O(\delta x/v_{\max})$ (assuming the interior solver has a CFL condition of this nature), this condition will almost certainly be satisfied in practice.

2.4 Stability

The stability of the method is readily proved. The main reason that the algorithm is stable is simply that it is dissipative: the filtering operator $(1 - \mathcal{O}_j^{\pm})$ has norm bounded by 1 and can therefore not increase the norm of $\vec{u}(x,t)$. Additionally, all dissipation occurs only at discrete instants of time, which minimizes interactions with the propagator. Using these ideas, it is straightforward to prove that the algorithm is stable, under the sole assumption that the interior propagator and the boundary conditions applied at the terminations of the buffer zones are stable.

Theorem 1 *The Time Dependent Phase Space Filtering propagation algorithm is stable if the interior solver is. In particular, we have the estimate:*

$$\|\vec{u}_d(x,t)\|_{L^2} \leq \|\vec{u}_0(x)\|_{L^2} \tag{2.11}$$

Proof. The idea of the proof is to show that the numerical solution operator at time t can be written as the product of operators of norm 1. Thus energy (L^2 norm) at time t must be bounded by the initial energy.

Define the operator U by:

$$U = \left[\prod_{j=1}^{N}(1 - \mathcal{O}_j^{+})(1 - \mathcal{O}_k^{-})\right] e^{\mathcal{H}_b T_{\text{step}}},$$

At time $t = mT_{\text{step}} + \tau$ (with $\tau \in [0, T_{\text{step}}]$), we can write the numerical solution $\vec{u}_d(x,t)$ as:

$$\vec{u}_d(x,t) = e^{\mathcal{H}_b \tau} U^m \vec{u}_0(x)$$

By the self-adjointness of $\mathcal{H}_b$, $\left\|e^{\mathcal{H}_b t}\right\| = 1$. If we can show that $\left\|1 - \mathcal{O}_k^{\pm}\right\| \leq 1$, then $\|U\| \leq 1$, implying:

$$\|\vec{u}_b(x,t)\|_{L^2} \leq \left\|e^{\mathcal{H}_b \tau}\right\| \|U\|^m \|\vec{u}_0(x)\|_{L^2} \leq 1 \cdot 1^m \cdot \|\vec{u}_0(x)\|_{L^2} = \|\vec{u}_0(x)\|_{L^2}$$

and stability is proved.

We first show that $\sigma(\mathcal{O}_j^{\pm}) \subseteq [0,1]$. Recall that $\mathcal{O}_j^{\pm}$ is defined as $\mathcal{O}_j^{\pm} = \chi_j^{\pm}(x) D^{\dagger} P(\vec{k}) D \chi_j^{\pm}(x)$. Note that $D^{\dagger} P(\vec{k}) D$ is diagonalizable (to $P(\vec{k})$) and

each diagonal entry is contained in $[0,1]$ for each $\vec{k}$. Therefore, $\left\|D^\dagger P(\vec{k})D\right\| \leq 1$ and $\sigma(D^\dagger P(\vec{k})D) = \sigma(P(\vec{k})) \in [0,1]$. This implies that $\left\|\mathcal{O}_j^\pm\right\| \leq 1$. Now write:

$$\begin{aligned}\left\langle f|\mathcal{O}_j^\pm f\right\rangle &= \left\langle \chi_j^\pm(x)f(x)|D^\dagger P(\vec{k})D\chi_j^\pm(x)f(x)\right\rangle \\ &= \left\langle D\chi_j^\pm(x)f(x)|P(\vec{k})D\chi_j^\pm(x)f(x)\right\rangle = \left\langle g|P(\vec{k})g\right\rangle\end{aligned}$$

where $g = D\chi_j^\pm(x)f(x)$. Since $P(\vec{k})$ is a positive matrix for each $\vec{k}$, positivity follows. Since $\mathcal{O}_j^\pm$ is a positive operator with norm bounded by 1, $\mathcal{O}_j^\pm$ has spectrum in $[0,1]$. The spectral mapping theorem implies that $\sigma(1-\mathcal{O}_j^\pm) \subseteq 1-[0,1] = [0,1]$, implying that $\left\|1-\mathcal{O}_j^\pm\right\| \leq 1$, and stability is proved. □

2.5 Tangential Waves and Evanescent Waves

The filter described in this section is not optimal. In particular, some outgoing waves that should be filtered are not, primarily waves which are outgoing, but nearly tangentially to the boundary or slowly decaying evanescent modes.

While it is impossible to completely resolve this issue (due to the uncertainty principle), one can improve the situation by using a better phase space localization scheme. One can build phase space projections using framelets (localized wavepackets) fine tuned to the problem of interest. For the Schrödinger equation, canonical coherent states (the Gaussian Windowed Fourier transform) frame [34] is a natural choice. A complete error analysis for such a method is presented in [36]. Hyperbolic equations as condidered here require different frames such as curvelets, wave atoms or Gaussian beams [10, 13, 28], and it seems likely that the analysis in [36] could be extended to the hyperbolic case using methods built on these. However, the simpler approach considered here may be preferable. In a later work we hope to present a more detailed study of the efficiency of the proposed method and the potential advantages of using different filter constructions.

3 Examples

All the tests considered used periodic boundary conditions and are solved by a FFT method. However, other numerical schemes can also be integrated into the phase space filter algorithm, and therefore, this would work for the nonlinear equations and linearizations around general nonconstant media.

3.1 Euler equations, linearized around a uniform mean flow

We consider now the two-dimensional Euler equations linearized around a uniform mean flow in the x_1 direction. (The simulation of this example is available

on Youtube.) The vector $\vec{u}(x,t)$ is 3 dimensional, with $\vec{u}_1$ representing the pressure change, $\vec{u}_{2,3}$ representing the velocity field in the $x_{1,2}$ directions (respectively). In this case, $\mathcal{H}$ takes the form:

$$\mathcal{H} = \begin{bmatrix} M\partial_{x_1} & -\partial_{x_1} & -\partial_{x_2} \\ -\partial_{x_1} & M\partial_{x_1} & 0 \\ -\partial_{x_2} & 0 & M\partial_{x_1} \end{bmatrix} \tag{3.1}$$

Here, $0 \leq M < 1$ is the Mach number. $\mathcal{H}$ has eigenvalues $\omega_1(\vec{k}) = Mk_1 + |\vec{k}|$, $\omega_2(\vec{k}) = Mk_1 - |\vec{k}|$ and $\omega_3(\vec{k}) = Mk_1$. The diagonalizing matrix is

$$D = \frac{1}{\sqrt{2}|\vec{k}|} \begin{bmatrix} -|\vec{k}| & k_1 & k_2 \\ |\vec{k}| & k_1 & k_2 \\ 0 & -\sqrt{2}k_1 & \sqrt{2}k_2 \end{bmatrix}. \tag{3.2}$$

When $M \neq 0$, this is the classical example of an equation for which the PML becomes unstable [23]. Although it has been shown how to restore stability for PML and CRBC in the case of flows in a duct [17, 19], as mentioned in the introduction these constructions have not been fully generalized to the three-dimensional case.

We solved the Euler equations for $M = 0.5$ on the region $[-32, 32]^2$ with lattice spacing $\delta x = 0.125$ (for a total of 512^2 lattice points). Such a setup is valid for spatial frequencies up to $k_{\max} = \pi/\delta x = 25.1$. We solved the system using the Fast Fourier transform to compute (1.3), which is accurate to machine precision provided no waves reach the boundary ([35, Theorem A.1]). This accuracy is independent of time-step, which we took to be $\delta t = 0.25$ in order to get a watchable frame-rate in the plots. The phase space filter region was taken to have width 16 (128 lattice points), with $T_{\text{step}} = 1.5$, and $\sigma = 1.0$. The initial condition was taken to be

$$u_1(x, t = 0) = r^2 e^{-r^2/9} \cos(Kr) \tag{3.3a}$$

with

$$r = \sqrt{(x-8)^2 + y^2}. \tag{3.3b}$$

with the K varying from 1 to 20 (the frequency range of the problem). This yields an initial condition with frequency localized near $|\vec{k}| = K$. The results were compared to another simulation on a large box. The result is that for $K > 4$, L^2 error of 10^{-3} (relative to the initial condition) is achieved up to $t = 50$ (see Figure 2). The error at low frequencies can be dealt with by various means, see Section 4 and [35].

We also vary the values of the parameter M and solved the Euler equations for $M = 0.1$ and 0.9 on the region $[-32, 32]^2$ with lattice spacing $\delta x = 0.125$ and show the results in Figures 3 and 4.

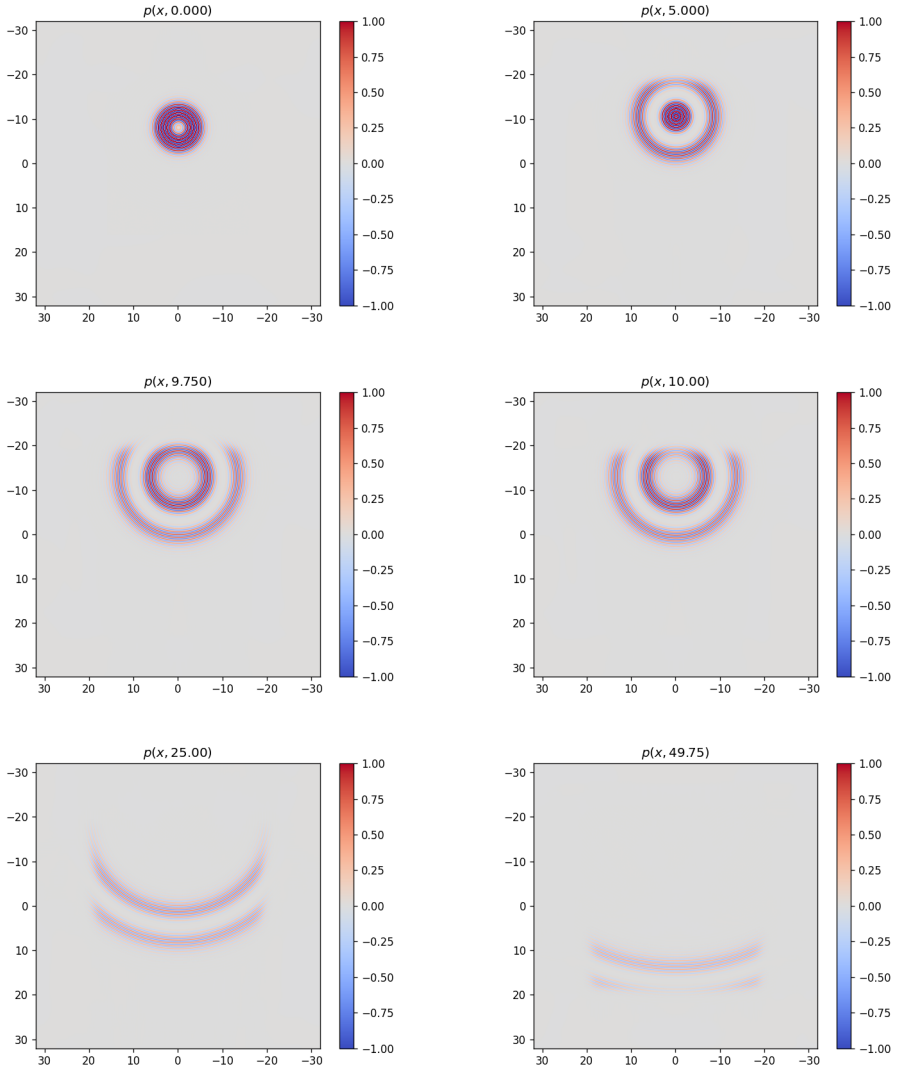

Figure 1: The pressure field at various times for $M = 0.5$. Note that the phase space filter was applied between $t = 9.75$ and $t = 10.0$.

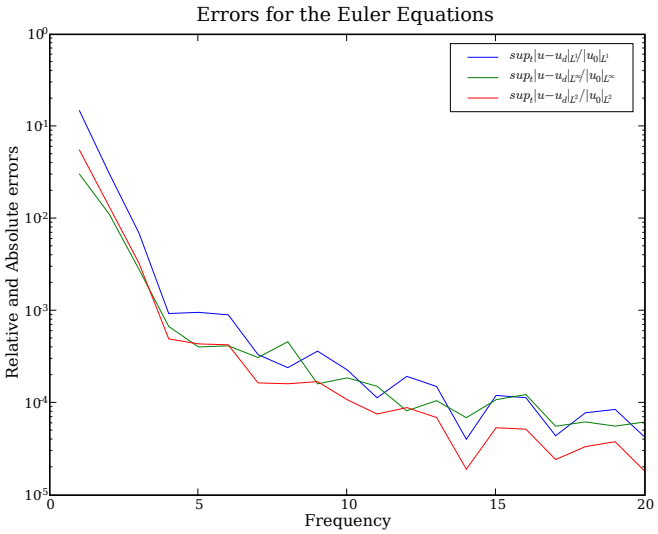

Figure 2: The relative error (measured in various norms) for $M = 0.5$ as a function of the frequency of the initial condition.

3.2 Maxwell's Equations in an Orthotropic Medium

Let $\vec{E}$ be the electric field and $\vec{H} = \mu\vec{B}$ with $\vec{B}$ the magnetic field. Let ϵ and μ be the electrical and magnetic permeability's of a medium.

In order to bring Maxwell's equations to symmetric form, we introduce the auxiliary variable $\vec{u} = (\sqrt{\mu}\vec{H}, \sqrt{\epsilon}\vec{E})^T$. With this formulation, the Hamiltonian for Maxwell's equations can be written in block form:

$$\mathcal{H} = \begin{bmatrix} 0 & -\mu^{-1/2}\nabla\times\epsilon^{-1/2} \\ \epsilon^{-1/2}\nabla\times\mu^{-1/2} & 0 \end{bmatrix} \tag{3.4}$$

where $\nabla\times$ is interpreted as a matrix,

$$\nabla\times = \begin{bmatrix} 0 & -\partial_z & \partial_y \\ \partial_z & 0 & -\partial_x \\ -\partial_y & \partial_x & 0 \end{bmatrix}.$$

The symmetry of ϵ, μ and $\nabla\times$ implies that $\mathcal{H}$ is skew-adjoint.

To further simplify the system, we make the following additional assumptions. We assume $\mu = 1$. We assume the system is z-independent, i.e. $\partial_z = 0$, and we can restrict ourselves to two-dimensional simulations. Lastly, we simplify the electrical permittivity:

$$\epsilon = \begin{bmatrix} 1 & b & 0 \\ b & 1 & 0 \\ 0 & 0 & c \end{bmatrix} \tag{3.5}$$

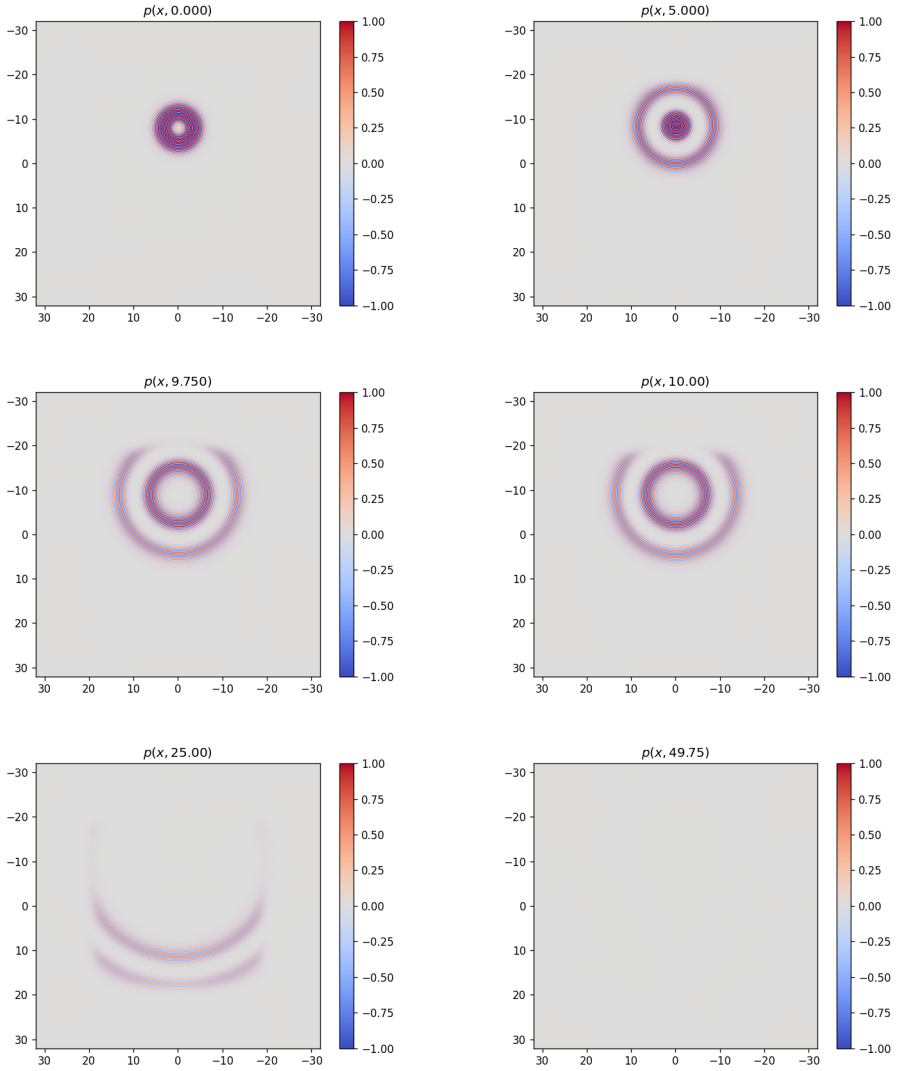

Figure 3: The pressure field at various times for $M = 0.1$. Note that the phase space filter was applied between $t = 9.75$ and $t = 10.0$.

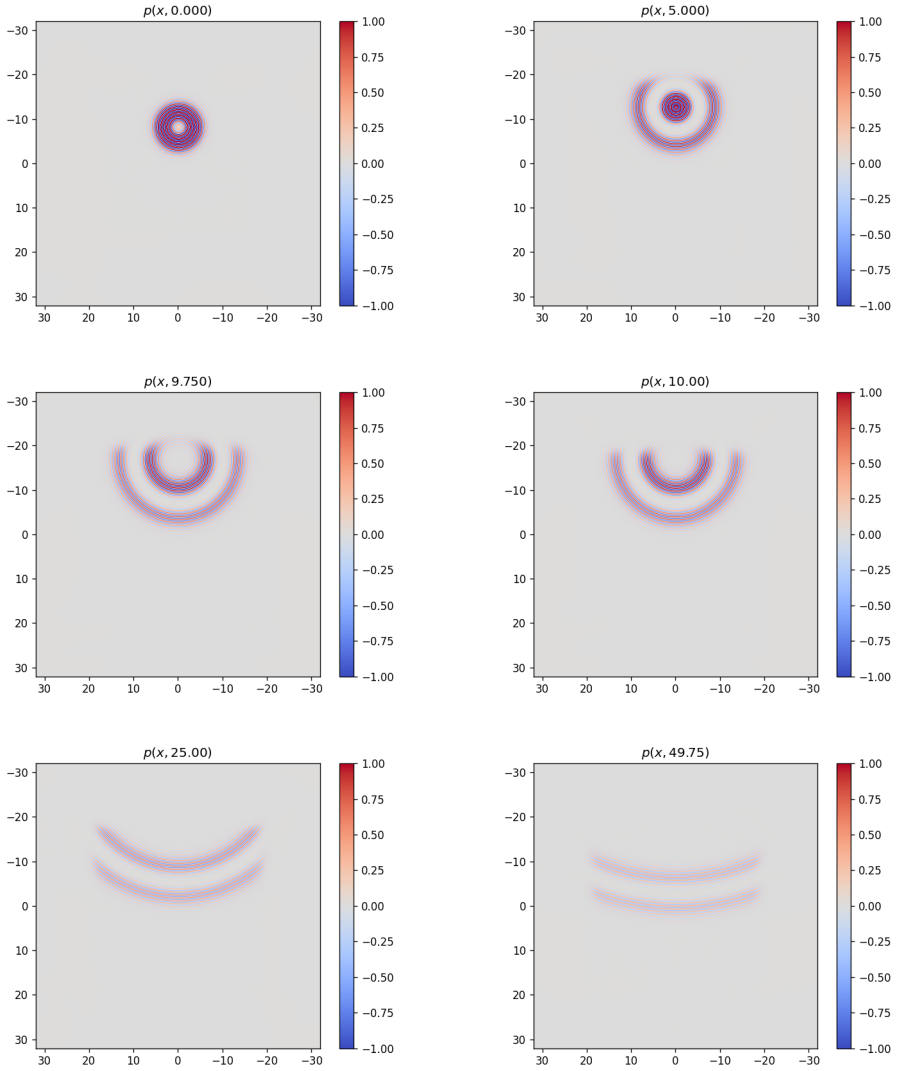

Figure 4: The pressure field at various times for $M = 0.9$. Note that the phase space filter was applied between $t = 9.75$ and $t = 10.0$.

This is the simplest possible birefringent system. With the variables

$$\begin{aligned} f &= (1/2)(\sqrt{1+b}+\sqrt{1-b}) \\ g &= (1/2)(-\sqrt{1+b}+\sqrt{1-b}), \end{aligned}$$

we can write the dispersion relation as:

$$\omega_{j=1,2}(\vec{k}) = (-1)^{1+j} i c^{-1} |\vec{k}| \tag{3.6a}$$

$$\omega_{j=3,4}(\vec{k}) = (-1)^{1+j} i \sqrt{(f^2+g^2)(k_1^2+k_2^2) - 4fgk_1k_2} \tag{3.6b}$$

$$\omega_{j=5,6}(\vec{k}) = 0. \tag{3.6c}$$

with

$$D = \begin{bmatrix} \frac{-k_2}{\sqrt{2}|\vec{k}|} & \frac{k_1}{\sqrt{2}|\vec{k}|} & 0 & 0 & 0 & 2^{-1/2} \\ \frac{k_2}{\sqrt{2}|\vec{k}|} & \frac{-k_1}{\sqrt{2}|\vec{k}|} & 0 & 0 & 0 & 2^{-1/2} \\ 0 & 0 & -2^{-1/2} & -\frac{fk_2-gk_1}{\sqrt{2}E(\vec{k})} & \frac{fk_1-gk_2}{\sqrt{2}E(\vec{k})} & 0 \\ 0 & 0 & 2^{-1/2} & -\frac{fk_2-gk_1}{\sqrt{2}E(\vec{k})} & \frac{fk_1-gk_2}{\sqrt{2}E(\vec{k})} & 0 \\ k_1\left|\vec{k}\right|^{-1} & k_2\left|\vec{k}\right|^{-1} & 0 & 0 & 0 & 0 \\ 0 & 0 & 0 & \frac{fk_1-gk_2}{E(\vec{k})} & \frac{fk_2-gk_1}{E(\vec{k})} & 0 \end{bmatrix} \tag{3.7}$$

with $E(\vec{k}) = \sqrt{(f^2+g^2)(k_1^2+k_2^2) - 4fgk_1k_2}$.

This can be further simplified by noting that u_1, u_2 and u_6 (corresponding to B_x, B_y, E_z are uncoupled to u_3, u_4 and u_5. The u_1, u_2 and u_6 modes (corresponding to B_x, B_y and E_z) are actually isotropic waves, so we will ignore them. We therefore restrict consideration to u_3, u_4 and u_5 (u_3 corresponds to B_z, and $u_{4,5}$ correspond to to linear combinations of E_x and E_y).

We solved the reduced system of Maxwell's equations with the same parameters as in Section 3.1, with the same initial condition (replacing u_1 by u_3 in (3.3a)). The anisotropy parameter b was chosen to be 0.25. The results are comparable to those for the Euler equation, see Figures 5 and 6.

We also vary the values of the parameter b and solved the equations for $b = 0.5$ and 0.75. Those results are displayed in Figures 7 and 8.

3.3 Long Time Stability

In Theorem 1 of Section 2.4, it was proved that the phase space filtering algorithm is stable. To demonstrate the validity of the theorem, we ran a simulation of the Euler equations and Maxwell's equations up to time $t = 2000$. While we can not determine the accuracy over such long time intervals (the reference simulation would require an extremely large box), we can study the growth of the L^2-norm.

The results of such a simulation are plotted in Figure 9. They indicate that Theorem 1 is correct, and that the mass of the solution decreases monotonically with time.

The simulation of this example is available on Youtube.

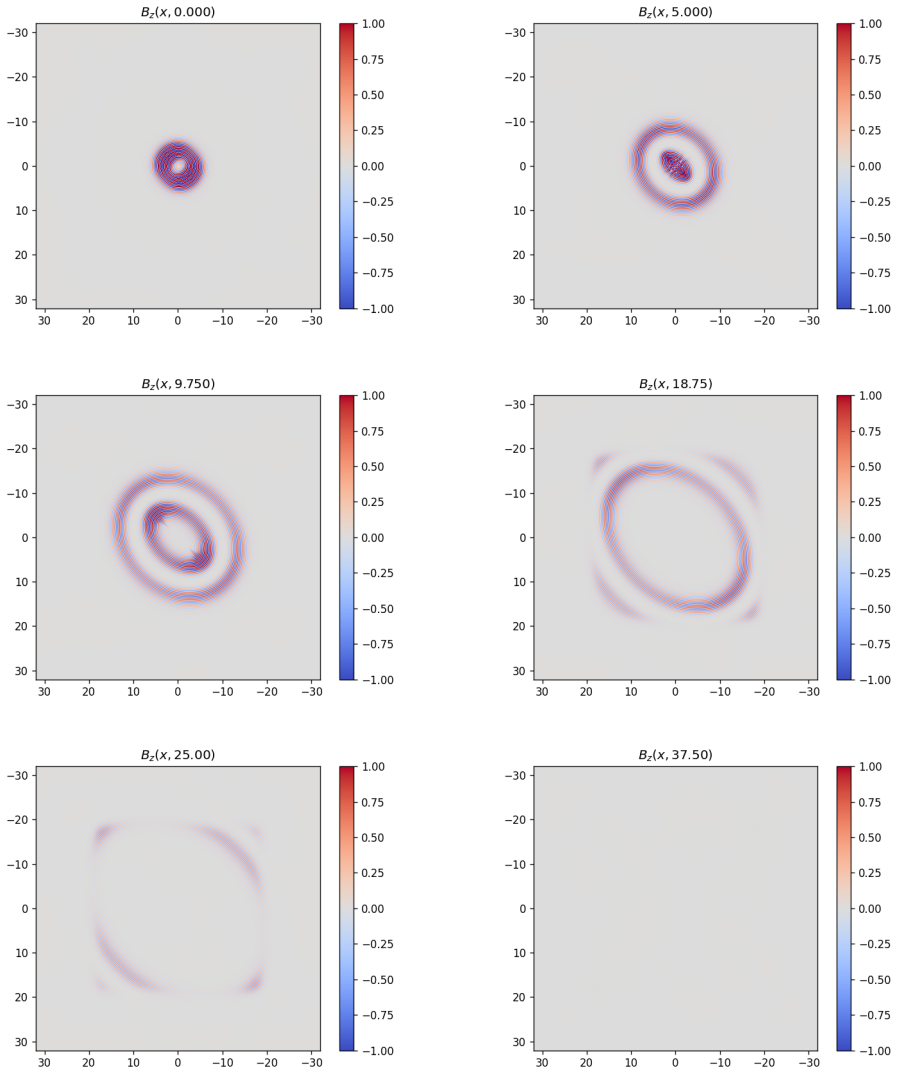

Figure 5: The magnetic component B_z of the electromagnetic pulse at various times for $b = 0.25$. Note that the phase space filter was applied between $t = 9.75$ and $t = 10.0$. The non-radial shape of the wave is due to the anisotropy of the medium.

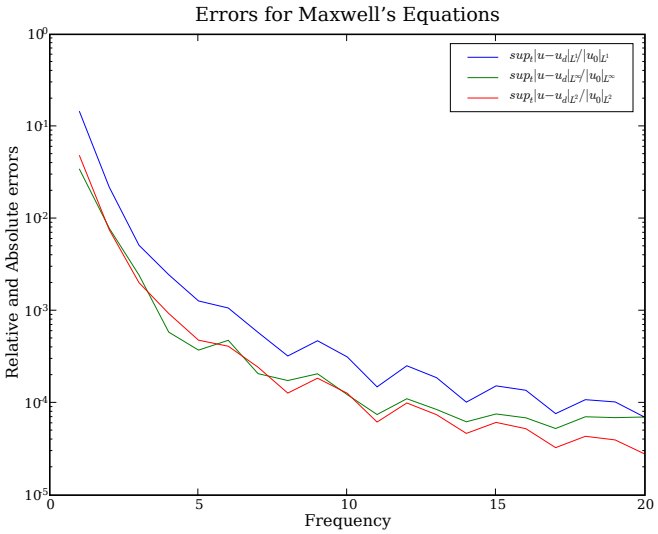

Figure 6: The relative error (measured in various norms) as a function of the frequency of the initial condition for $b = 0.25$.

4 The Low Frequency Problem

As is apparent from Figures 2 and 6, the phase space filtering approach does not work well for waves with low frequency. The reason for this is that to localize in frequency, the region in which one works must be $O(1)$ wavelengths long. The simplest remedy is to increase the width of the filter. If the smallest frequency relevant to the problem is k_b, then the width of the buffer is $O({k_b}^{-1})$, which means that the computational cost is of order $O({k_b}^{-N})$.

This problem can be remedied by a somewhat more involved method, which has been implemented for the Schrödinger equation [35]. The essential idea is to increase the width of the box, but reduce the sampling rate on the extended region. Then high frequency waves are filtered at the edge of the highly sampled region, and low frequency waves are filtered on the edge of the coarsely sampled region, but using a wider filter capable of resolving low frequency waves.

With this method, even though the computational box has width $O({k_b}^{-1})$, the number of samples required is only $O(\log(k_{\max}/k_b))$ (computation time scales similarly, up to logarithmic prefactors). This allows resolution of outgoing waves at low frequencies in logarithmic rather than linear cost. It is also argued heuristically in [35] that this computational complexity is close to the best possible. As an illustration, we apply this method to the 1-dimensional Schrödinger equation. The results are plotted in Figure 10, and the full details of the algorithm are described in [35].

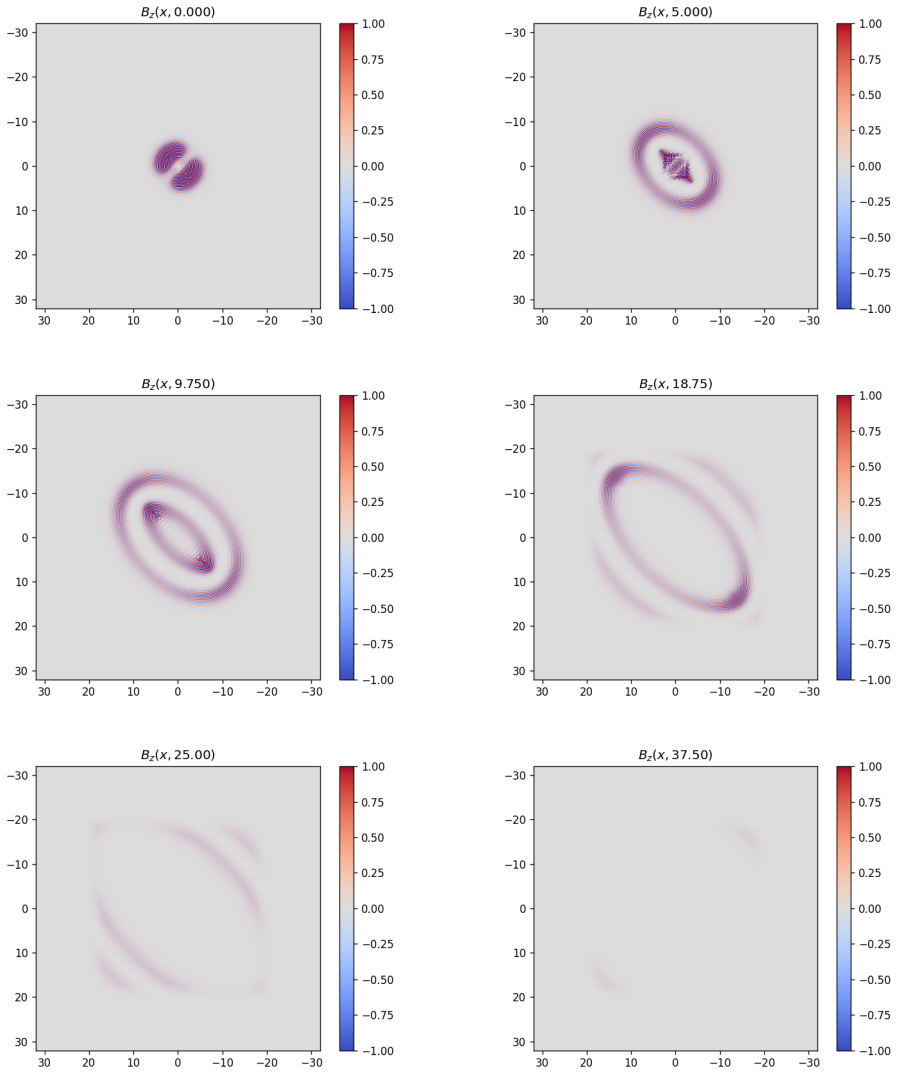

Figure 7: The magnetic component B_z of the electromagnetic pulse at various times for $b = 0.5$. Note that the phase space filter was applied between $t = 9.75$ and $t = 10.0$. The non-radial shape of the wave is due to the anisotropy of the medium.

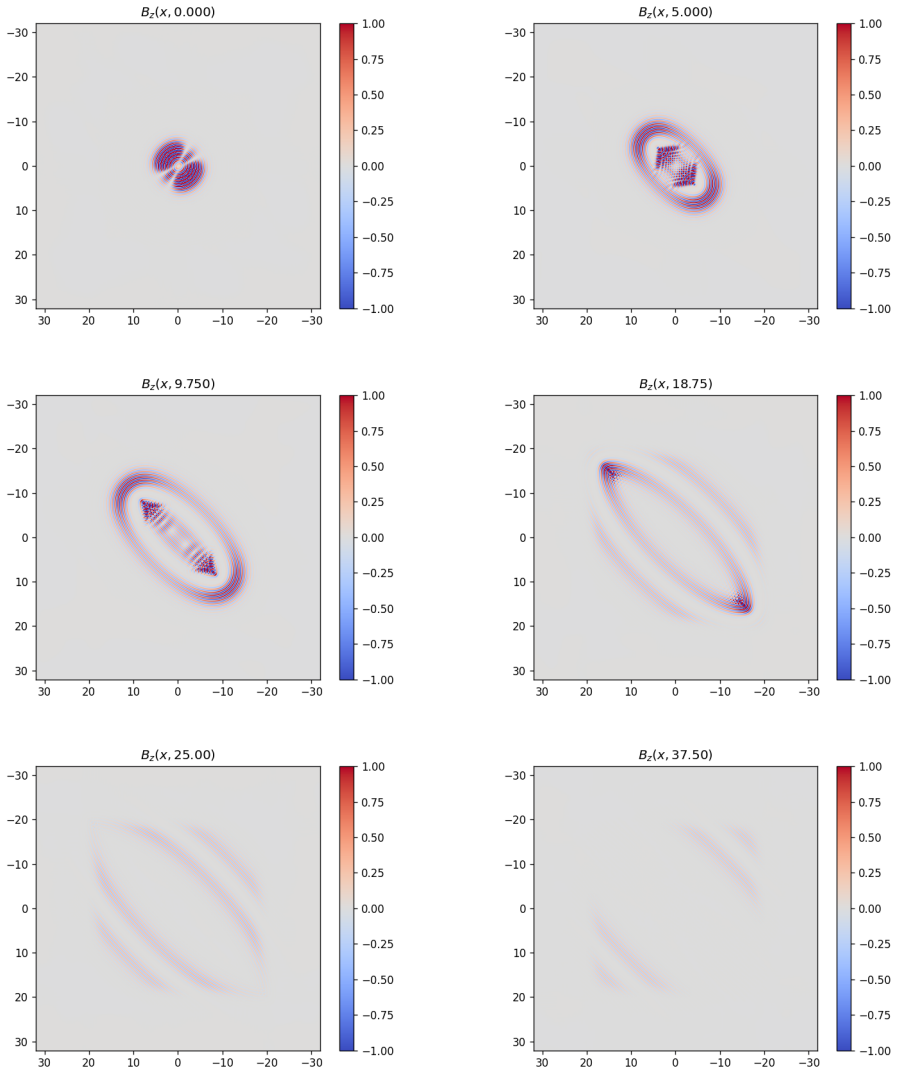

Figure 8: The magnetic component B_z of the electromagnetic pulse at various times for $b = 0.75$. Note that the phase space filter was applied between $t = 9.75$ and $t = 10.0$. The non-radial shape of the wave is due to the anisotropy of the medium.

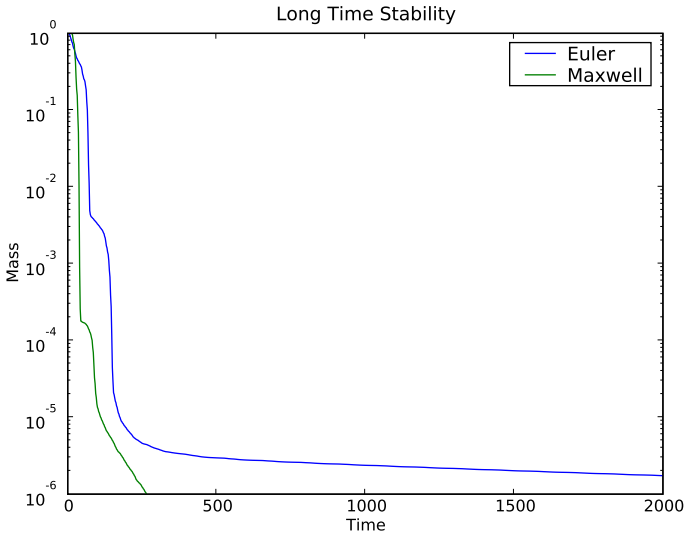

Figure 9: The L^2 norm of solutions of the Euler and Maxwell equations as a function of time. In both cases, we took $K = 10$ (recall (3.3a)). The Mach number was $M = 0.5$ for the Euler equations and the anisotropy was $b = 0.25$ for Maxwell's equations.

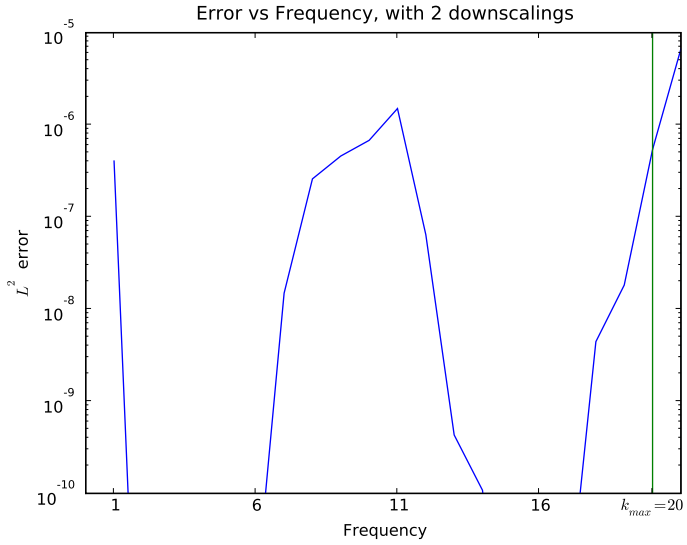

Figure 10: A graph of error vs frequency for the multiscale method described in this section. The grid was downscaled twice, thus allowing the resolution of waves with frequencies as low as $k = 1$. The details of this computation are given in [35, Section 5.1].

5 Conclusion

In summary, we have demonstrated the application to hyperbolic systems of a general-purpose method for solving wave propagation problems on unbounded domains. To our knowledge, this is the only mathematically-justifed method which is stable and convergent for arbitrary systems. The focus of future developments will be:

- Optimization of efficiency and applications of the multiscale approach: in particular we will consider the question of how to best scale a hierarchy of buffers to minimize the degrees-of-freedom in the buffer zone. Alternatives such as including grid stretching will be considered.
- A detailed error analysis of the simpler Gaussian filters considered here and comparisons with more elaborate methods based on multiscale wave representations.

References

[1] B. Alpert, L. Greengard, and T. Hagstrom. Rapid evaluation of nonreflecting boundary kernels for time-domain wave propagation. *SIAM J. Numer. Anal.*, 37:1138–1164, 2000.

[2] B. Alpert, L. Greengard, and T. Hagstrom. Nonreflecting boundary conditions for the time-dependent wave equation. *J. Comput. Phys.*, 180:270–296, 2002.

[3] D. Appelö and T. Colonius. A high-order super-grid-scale absorbing layer and its application to linear hyperbolic systems. *J. Comput. Phys.*, 228:4200–4217, 2009.

[4] D. Appelö, T. Hagstrom, and G. Kreiss. Perfectly matched layers for hyperbolic systems: General formulation, well-posedness and stability. *SIAM J. Appl. Math.*, 67:1–23, 2006.

[5] E. Bécache, S. Fauqueux, and P. Joly. Stability of perfectly matched layers, group velocities, and anisotropic waves. *J. Comput. Phys.*, 188:399–433, 2003.

[6] E. Bécache, S. Fliss, M. Kachanovska, and M. Kazakova. On a surprising instability result of Perfectly Matched Layers for Maxwell's equations in 3D media with diagonal anisotropy. *Comptes Rendus. Mathématique, Académie des sciences (Paris)*, (10.5802/crmath.165), 2021.

[7] E. Bécache, D. Givoli, and T. Hagstrom. High-order Absorbing Boundary Conditions for anisotropic and convective wave equations. *J. Comput. Phys.*, 229:1099–1129, 2010.

[8] J.-P. Bérenger. A perfectly matched layer for the absorption of electromagnetic waves. *J. Comput. Phys.*, 114:185–200, 1994.

[9] E. Bécache, P. Joly, and V. Vinoles. On the analysis of perfectly matched layers for a class of dispersive media and application to negative index metamaterials. *Math. Comp.*, 87:2775–2810, 2018.

[10] E. Candés and L. Demanet. The curvelet representation of wave propagators is optimal. *Comm. Pure and Appl. Math.*, 58:1472–1528, 2005.

[11] W. Chew and W. Weedon. A 3-D perfectly matched medium from modified Maxwell's equations with stretched coordinates. *Microwave Optical Technol. Lett.*, 7:599–604, 1994.

[12] I. Daubechies. Time-frequency localization operators: a geometric phase space approach. *IEEE Trans. Inform. Theory*, 34:605–612, 1988.

[13] L. Demanet and L. Ying. Wave atoms and time upscaling of wave equations. *Numer. Math.*, 113:1–71, 2009.

[14] K. Duru and G. Kreiss. A well-posed and discretely stable perfectly matched layer for elastic wave equations in second order formulation. *Commun. Comput. Phys.*, 11:1643–1672, 2012.

[15] M. Ehrhardt and C. Zheng. Exact artificial boundary conditions for problems with periodic structures. *J. Comput. Phys.*, 227:6877–6894, 2008.

[16] S. Graffi and K. Yajima. Exterior complex scaling and the ac-stark effect in a coulomb field. *Commun. Math. Phys.*, 89:277–301, 1983.

[17] T. Hagstrom. Perfectly matched layers for hyperbolic systems with applications to the linearized Euler equations. In G. Cohen, P. Joly, E. Heikkola, and P. Neittaanmäki, editors, *Mathematical and Numerical Aspects of Wave Propagation Phenomena*, pages 125–129. Springer-Verlag, 2003.

[18] T. Hagstrom. Extensions of complete radiation boundary conditions to dispersive waves. In *Waves 2017*, pages 175–176, 2017.

[19] T. Hagstrom, E. Bécache, D. Givoli, and K. Stein. Complete radiation boundary conditions for convective waves. *Commun. in Comput. Phys.*, 11:610–628, 2012.

[20] T. Hagstrom, S.I. Hariharan, and D. Thompson. High-order radiation boundary conditions the convective wave equation in exterior domains. *SIAM J. Sci. Comput.*, 25:1088–1101, 2003.

[21] T. Hagstrom and T. Warburton. Complete radiation boundary conditions: minimizing the long time error growth of local methods. *SIAM J. Numer. Anal.*, 47:3678–3704, 2009.

[22] M. Halla, M. Kachynovska, and M. Weiss. Radial perfectly matched layers and infinite elements for the anisotropic wave equation. Submitted, 2024.

[23] F. Hu. On absorbing boundary conditions for linearized Euler equations by a perfectly matched layer. *J. Comput. Phys.*, 129:201–219, 1996.

[24] S. Jiang and L. Greengard. Efficient representation of nonreflecting boundary conditions for the time-dependent Schrödinger equation in two dimensions. *Commun. Pure and Appl. Math.*, 61:261–288, 2008.

[25] S. Lau. Rapid evaluation of radiation boundary kernels for time-domain wave propagation on blackholes: implementation and numerical tests. *Class. Quantum Grav.*, 21:4147–4192, 2004.

[26] S. Lau. Rapid evaluation of radiation boundary kernels for time-domain wave propagation on blackholes: theory and numerical methods. *J. Comput. Phys.*, 199:376–422, 2004.

[27] S. Parrish and F.. Hu. Pml absorbing boundary conditions for the linearized and nonlinear euler equations in the case of oblique mean flow. *International Journal for Numerical Methods in Fluids*, 60:565–589, 2009.

[28] J. Qian and L. Ying. Fast multiscale Gaussian wavepacket transforms and multiscale Gaussian beams for the wave equation. *Multiscale Model. Simul.*, 8:1803–1837, 2010.

[29] J. Rauch. *Hyperbolic Partial Differential Equations and Geometric Optics*, volume 133 of *Graduate Studies in Mathematics*. American Mathematical Society, Providence RI, 2012.

[30] I. M. Sigal and A. Soffer. Asymptotic completeness of short-range many-body systems. *Bull. Amer. Math. Soc. (N.S.)*, 14:107–110, 1986.

[31] I. M. Sigal and A. Soffer. The N-particle scattering problem: asymptotic completeness for short-range systems. *Ann. of Math. (2)*, 126:35–108, 1987.

[32] I. M. Sigal and A. Soffer. Asymptotic completeness of N-particle long-range scattering. *J. Amer. Math. Soc.*, 7:307–334, 1994.

[33] B. Simon. Resonances and complex scaling: A rigorous overview. *Int. J. Quantum Chemistry*, page 529–542, 1978.

[34] A. Soffer and C. Stucchio. Open boundaries for the nonlinear schrödinger equation. *J. Comput. Phys.*, 225:1218–1232, 2007.

[35] A. Soffer and C. Stucchio. Multiscale resolution of shortwave-longwave interaction. *Commun. Pure and Appl. Math*, 62:82–124, 2009.

[36] A. Soffer, C. Stucchio, and M.-B. Tran. *Time Dependent Phase Space Filters: A Stable Absorbing Boundary Condition*. Springer Briefs on PDEs and Data Science. Springer Nature, Singapore, 2023.